Bone Diagenesis and Stratigraphy: Developing a Fossil-Bone Recontextualization Model in Pleistocene Karst Systems

Héctor Del Valle[1,2], Alejandro B. Rodríguez-Navarro[3], Abel Moclán[4,5], Paula García-Medrano[6,2,7,8], Isabel Cáceres[2,1]

[1] Institut Català de Paleoecologia Humana i Evolució Social (IPHES-CERCA), Tarragona, Spain.
[2] Universitat Rovira i Virgili, Tarragona, Spain.
[3] Universidad de Granada, Granada, Spain.
[4] PALEVOPRIM, Université de Poitiers and CNRS, Poitiers, France.
[5] Institute of Evolution in Africa (IDEA), University of Alcalá de Henares, Madrid, Spain.
[6] National Human Evolution Research Centre (CENIEH), Burgos, Spain
[7] UMR 7194 HNHP (MNHN-CNRS-UPVD), MNHN, Paris, France.
[8] British Museum, London, UK.

ATHENS American School of Classical Studies at Athens (ASCSA)

Héctor Del Valle
hdelvalle@iphes.cat

Introduction

Galería site is located in the Sierra de Atapuerca (Burgos, Spain) and comprises five lithostratigraphic units (GI–GV). Subunits GIIa, GIIb, GIIIa, GIIIb, and GIV correspond to the allochthonous infill containing abundant faunal and lithic remains, chronologically framed within the Middle Pleistocene (MIS10–MIS7) [1-3].

The site is interpreted as a natural trap, where hominins and carnivores exploited animals that fell into the cavity. In the 1970s, a human mandible, later attributed to *Homo heidelbergensis* [4], was recovered from the trench slope. However, its original stratigraphic context remains unknown, preventing further interpretation for decades.

In this work, we investigate diagenetic trajectories to assess preservation differences across the stratigraphic units [5]. Based on these results, we developed a machine learning model using diagenetic parameters to recontextualize the human mandible of Galería site.

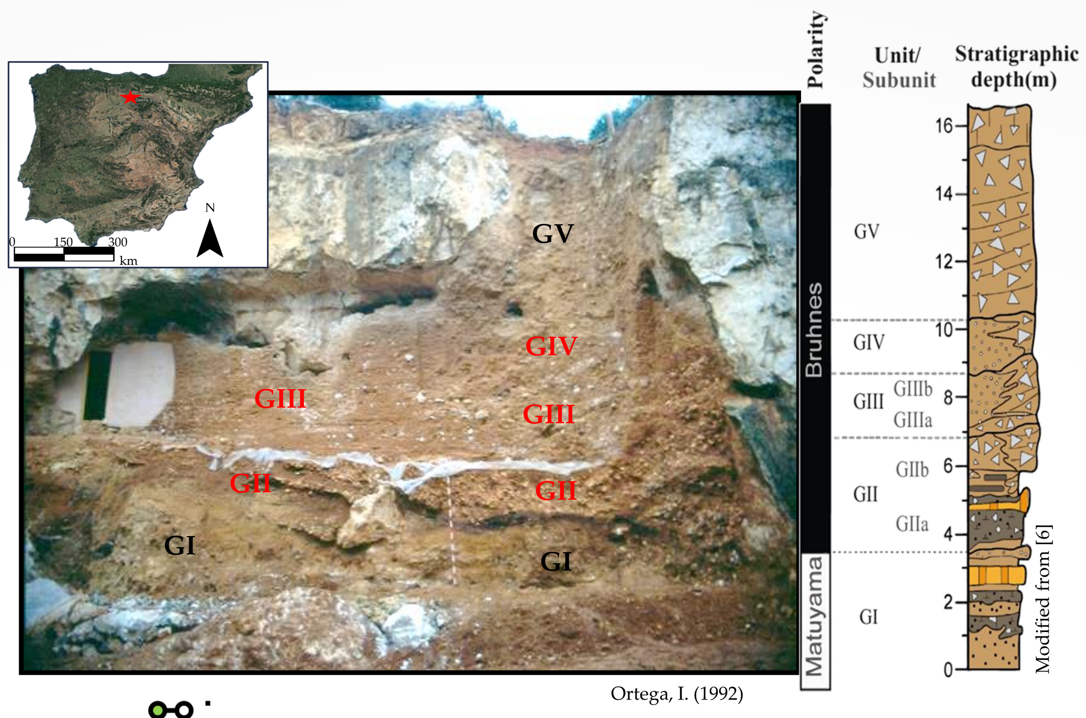

Ortega, I. (1992)

Material & Methods

We analyzed 150 cortical fossil bone samples from Galería (30 per stratigraphic unit, GIIa to GIV). **FTIR** provided eleven diagenetic parameters: phosphate indices (IRSF, FWHMv$_3$PO$_4$, 1118 and 1145 cm^{-1} in the deconvoluted spectra attributed to HPO$_4$; 1030 cm^{-1} and 960 cm^{-1} in the deconvoluted spectra attributed to highly and poorly crystalline phosphate, HCP and PCP; OH/PO$_4$ at 630/605) and carbonate indices (C/P at 1415/1010, C/C at 1455/1410, calcite/PO$_4$ at 712/1010). XRD yielded apatite unit cell parameters and cell volume, while TEM provided information of crystal sizes and morphologies. Assemblage differences were statistically assessed, and **PCA with correlation analyses** reduced multicollinearity. Selected variables trained **machine learning models in R**, enabling stratigraphic recontextualization of the human mandible.

Visit the paper

Results & Discussion

1.FTIR

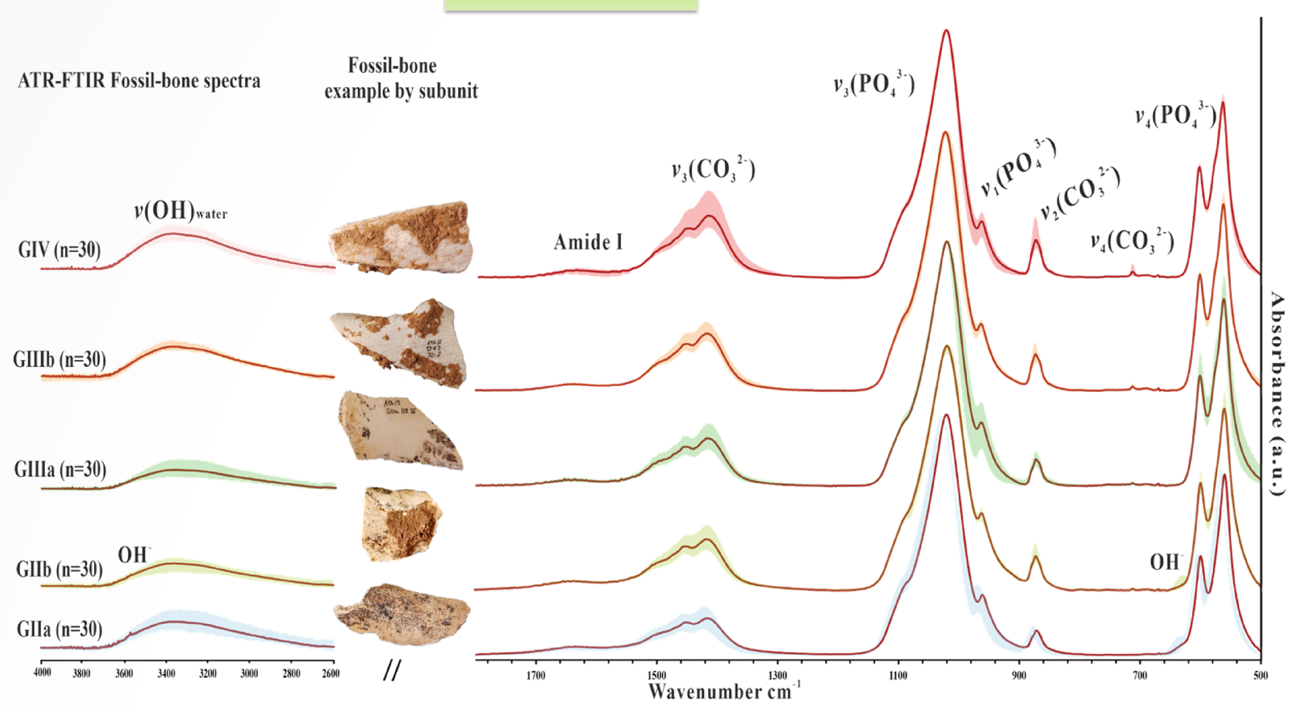

2.XRD

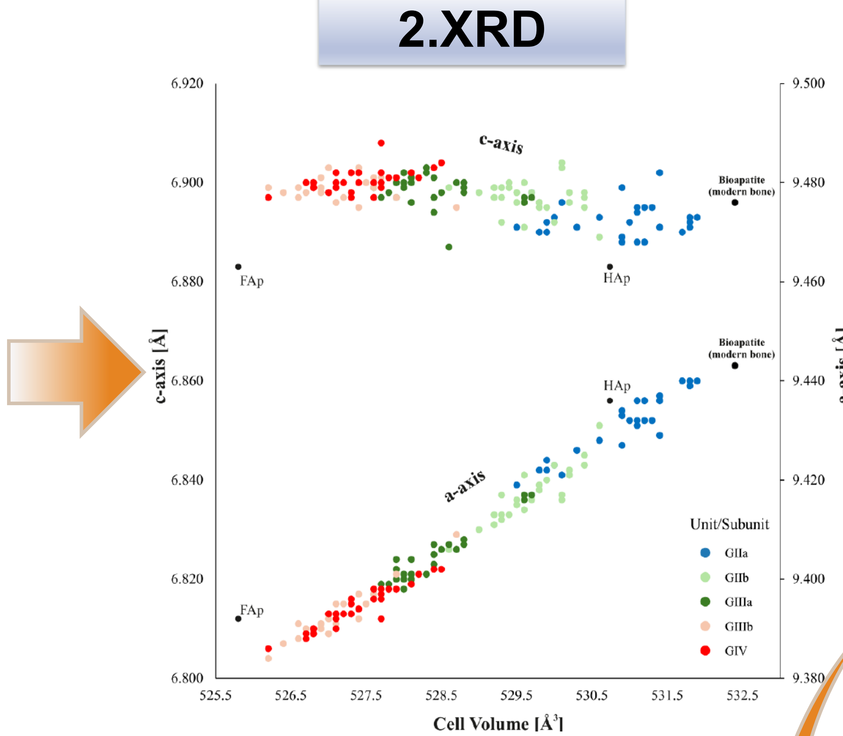

3. Back-calculated Parameters & Statistics

	GIIa	GIIb	GIIIa	GIIIb	GIV
IRSF	4.803 ± 0.386	4.362 ±0.281	4.242 ± 0.209	4.186 ±0.144	4.161 ± 0.134
FWHM$_{v_3PO_4}$	69.437 ± 4.111	72.962 ± 2.889	70.788 ± 4.052	68.850 ± 2.719	66.318 ± 2.768
PCP	0.028 ± 0.007	0.034 ± 0.008	0.028 ± 0.009	0.022 ± 0.007	0.018 ± 0.007
OH/PO$_4$	0.125 ± 0.078	0.019 ± 0.051	-	-	-
HPO$_4$1118	0.017 ± 0.002	0.017 ± 0.002	0.020 ± 0.002	0.021 ± 0.001	0.024 ± 0.002
HPO$_4$1145	0.270 ± 0.065	0.136 ± 0.043	0.082 ± 0.040	0.117 ± 0.020	0.066 ± 0.028
HCP	0.170 ± 0.018	0.148 ± 0.009	0.151 ± 0.006	0170 ± 0.010	0.181 ± 0.011
Calcite/PO$_4$	-	0.002 ± 0.005	0.003 ± 0.007	0.003 ± 0.008	0.013 ± 0.002
C/C	0.977 ± 0.093	0.843 ± 0.052	0.764 ± 0.048	0.785 ± 0.060	0.725 ± 0.048
C/P	0.138 ± 0.024	0.188 ± 0.027	0.194 ± 0.026	0.204 ± 0.022	0.226 ± 0.056
Amide I/PO$_4$	0.009 ± 0.002	0.010 ± 0.002	0.010 ±0.001	0.011 ± 0.001	0.013 ± 0.002
Cell volume (A^3)	530.9±0.7	529.7±0.5	528.5±0.9	527.1±0.5	527.4 ±0.6
a-axis (Å)	9.431±0.007	9.417±0.006	9.405±0.008	9.393±0.005	9.394 ± 0.004
c-axis (Å)	6.892±0.003	6.897 ±0.003	6.899±0.003	6.899±0.002	6.900 ± 0.002

5 parameters showed statistically significant differences without collinearity

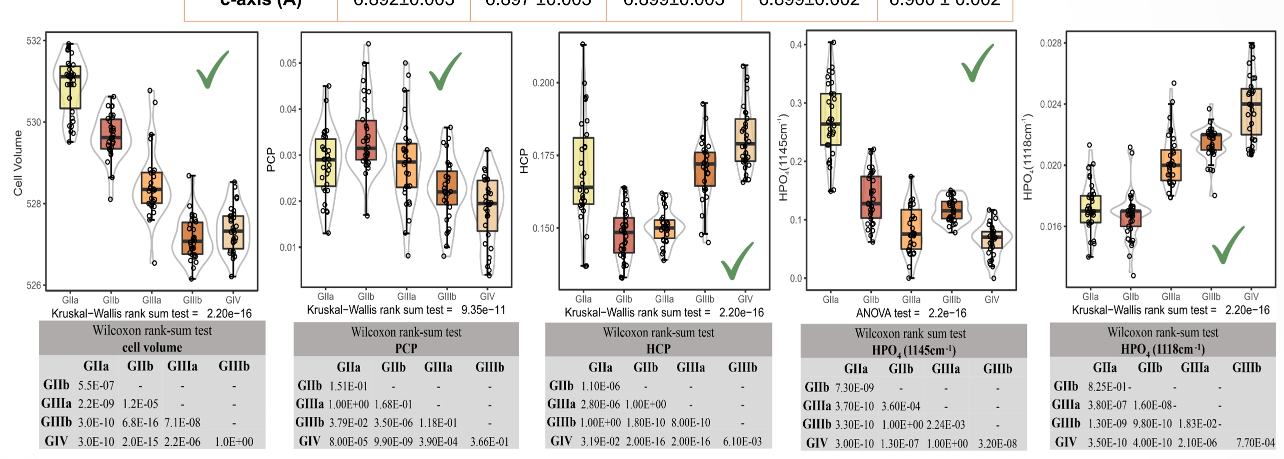

3.1 PCA

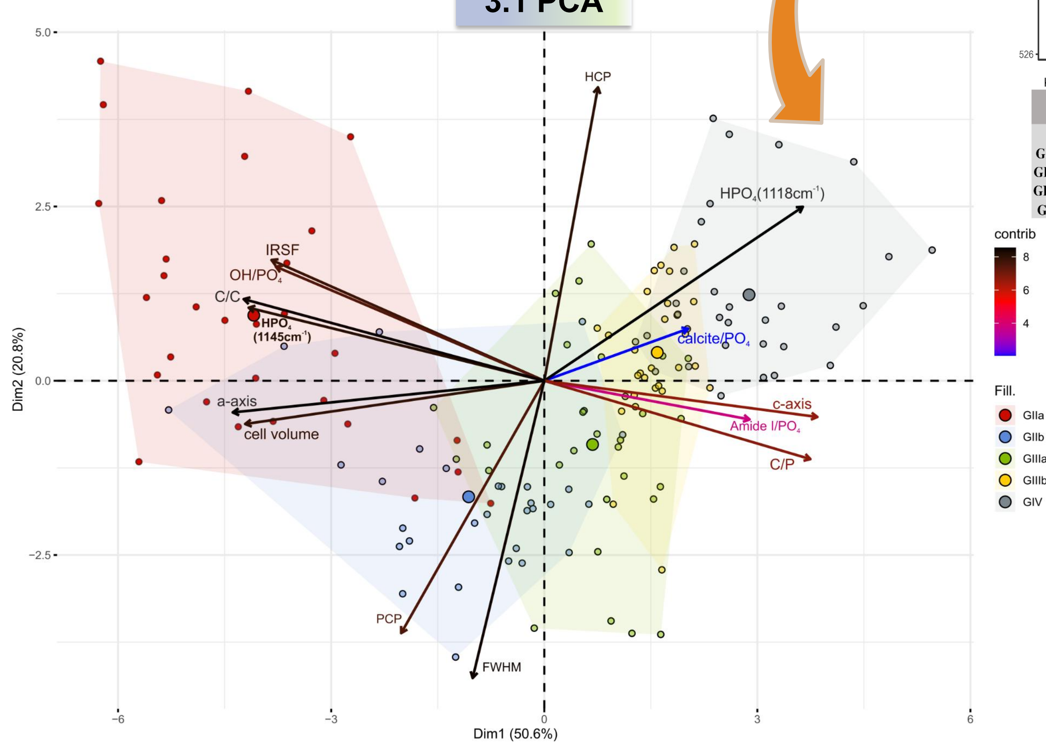

3.2 Machine learning

	NNET	SVM	KNN	RF	MDA	NB	LDA	PLS	DTC5.0
Accuracy	**0.89**	0.84	0.80	0.82	0.87	0.84	0.82	0.69	0.76
Kappa	**0.86**	0.81	0.75	0.78	0.83	0.81	0.78	0.61	0.69
acc lower	**0.76**	0.71	0.65	0.68	0.73	0.71	0.68	0.53	0.61
acc upper	**0.96**	0.94	0.90	0.92	0.95	0.94	0.92	0.82	0.87

Εὕρηκα!, NNET shows the best performance with five parameters.

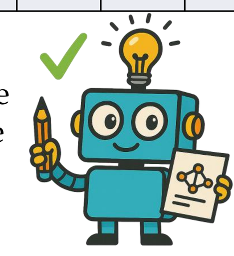

- **FTIR**: In GII, bones exhibited higher crystallinity (IRSF, HCP). Carbonate indices showed strong depletion in GIIa (low C/P), followed by an increase towards GIV. The C/C ratio decreased, indicating higher B-CO$_3$ in the upper units. Calcite was absent in GIIa but appeared clearly in GIV.
- **XRD**: There is a progressive reduction in the apatite unit cell volume from the oldest to the youngest levels. This trend reflects increasing F$^-$ incorporation into the apatite lattice up-sequence, with GII closer to HAp/CHAp and GIII–GIV approaching fluorine-containing apatites.
- **TEM**: Apatite nanocrystals are elongated and splintered in the lower units, but compact and thicker in the upper levels where fluorine is present.
- **Statistical analyses:** : There are significant differences between units. PCA and ML showed that the most important parameters for discrimination are related to phosphates and unit cell volume. The best-performing models were NNET and MDA.

Burial history overview

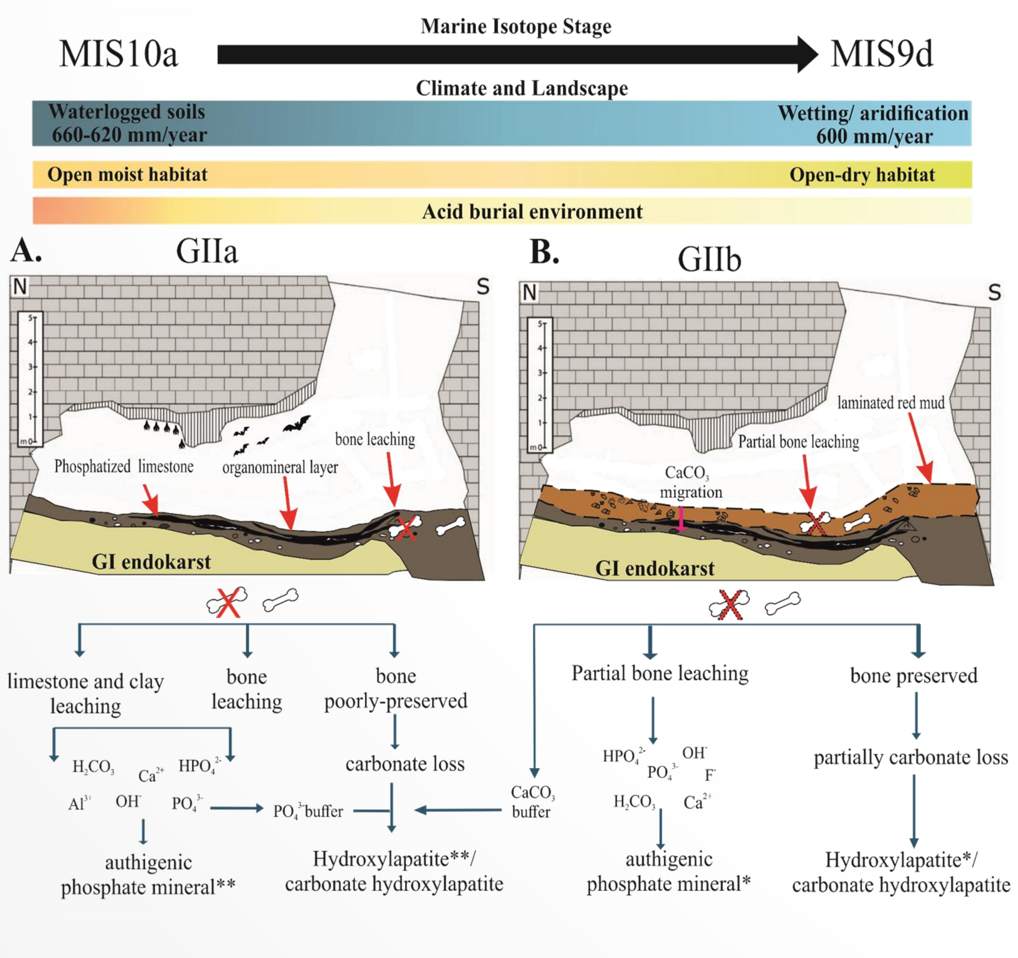

Crystalline phases evolved by dissolution–(re)precipitation processes. In the GII unit, acidic and wet conditions prevailed. In GIIa (A), leaching caused severe bone loss and authigenic phosphate minerals formation, with remains showing hydroxylapatite depleted in carbonate. In GIIb (B), drier conditions and CaCO$_3$ precipitation buffered pH, stabilizing carbonate hydroxylapatite and improving preservation. In the GIII–GIV units (MIS 9c–7e), environments became slightly alkaline, favoring calcite precipitation and fluorine substitution into bone apatite. From GIIIa (C) dissolution–(re)precipitation intensified, producing fluorine-rich apatite phases. The close diagenetic trajectories of GIIIb and GIV (D) suggest rapid sedimentation, leading to the final infilling of the cave.

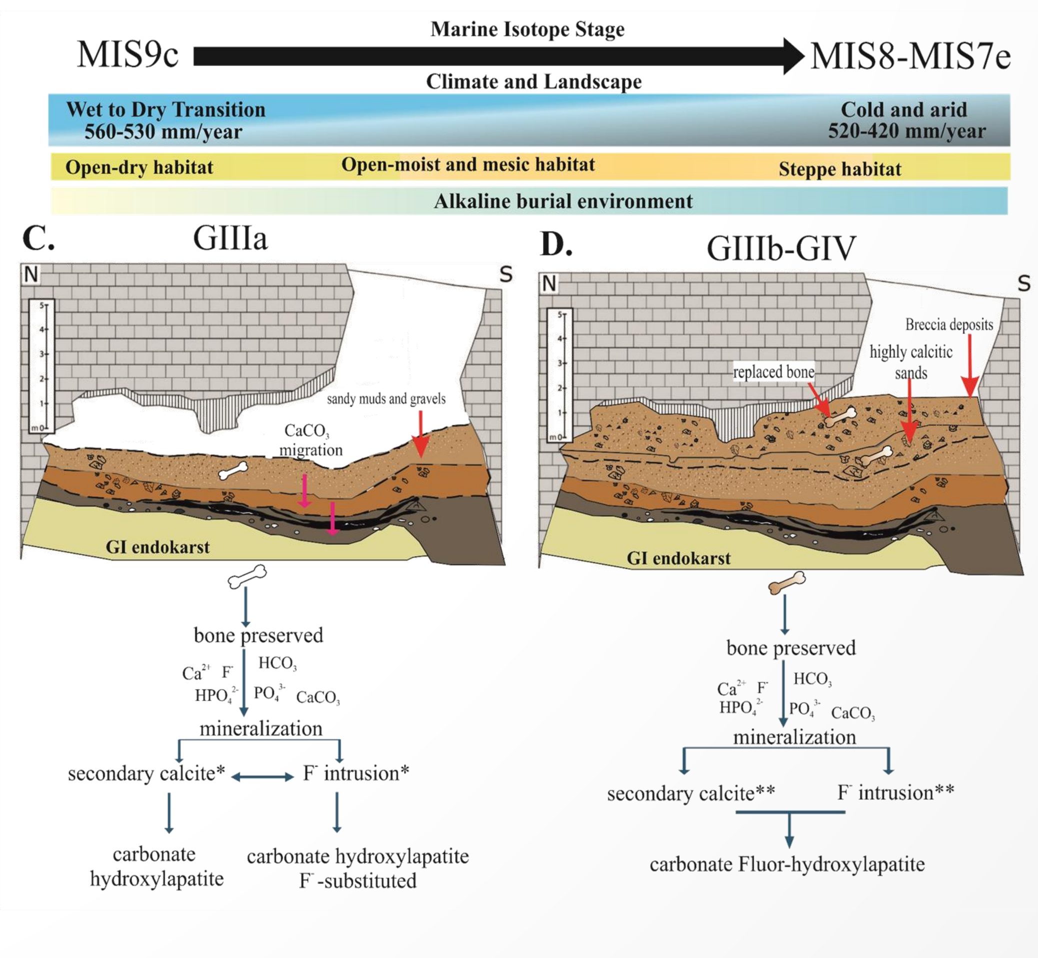

4. TEM

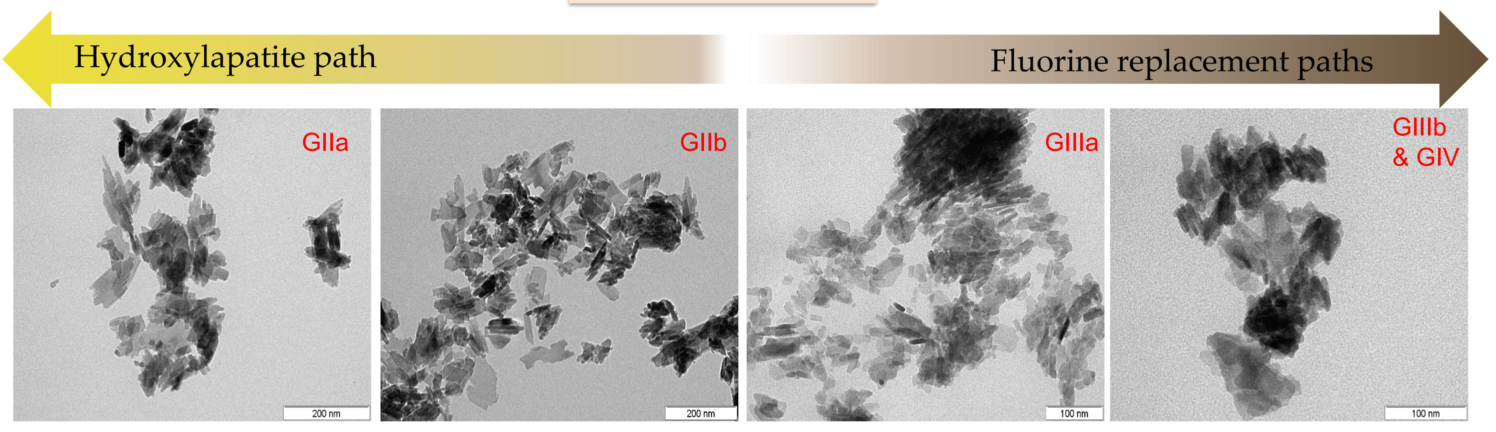

Then… Where are you from?

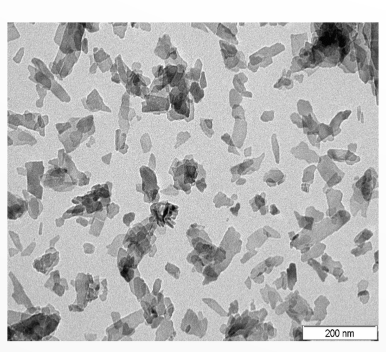

data for NNET
Cell volume [A^3] = 530.53±0.08
HPO$_4$1118 = 0.02±0.00
HPO$_4$1145 = 0.32±0.04
PCP = 0.04±0.00
HCP = 0.14±0.01

other data
IRSF = 4.75±0.06
C/P = 0.14±0.01

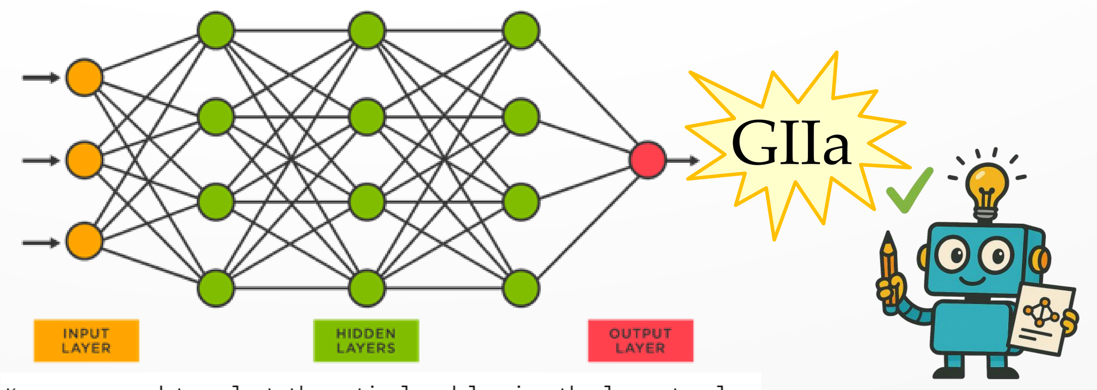


```
Kappa was used to select the optimal model using the largest value.
The final values used for the model were size = 5 and decay = 0.1.
> new_sample
  a1118 a1145    PCP   HCP    cell predicted_class
1 0.019  0.32 0.0403 0.144 530.526            GIIa
> probabilities
       GIIa       GIIb       GIIIa       GIIIb          GIV
1 0.8926714 0.07364779 0.03144103 0.002046593 0.0001932261
```

Final Remarks

The human mandible is assigned to unit GIIa with a probability of 0.9. This level dates to around 400 ka, making it contemporaneous with the Sima de los Huesos population (Burgos, Spain).

The main differences between units result from the adaptation of phosphate minerals to the burial environment. Dissolution–(re)precipitation processes modify nanocrystals along two main paths: one towards fluorine-containing apatites, and the other towards hydroxylapatites.

Thus, we propose a fossil recontextualization model based on bone diagenesis, stratigraphy, and machine learning, which is applicable to other archaeological sites.

Acknowledgments

This research is supported by: MCIN/AEI projects PID2021-122355NB-C32, PID2024-156477NB-C32, PID2020-116660GB-I00 and PRE2021-100275 (HDV); 2021SGR-01238 (AGAUR), 2023-PFR-URV-01238 (URV), LATEUROPE-ERC (101052653) at CNRS; and Fyssen Foundation (AM). The authors are thankful to the SRCiT of the URV and the Department of Mineralogy and Petrology of the UGR for their technical support and advice. We would also like to thank the Atapuerca team for their support, collaboration, and availability

References

[1] Berger, G.W.; Pérez-González, A.; Carbonell, E. et al. (2008). Luminescence chronology of cave sediments at the Atapuerca paleoanthropological site, Spain. Journal of Human Evolution, 55(2), 300–311. **[2]** Falguères, C.; Bahain, J.J.; Bischoff, J.L. et al. (2013). Combined ESR/U-series chronology of Acheulian hominid-bearing layers at Trinchera Galería site, Atapuerca, Spain. Journal of Human Evolution, 65(2), 168–184. **[3]** Demuro, M.; Arnold, L.J.; Parés, J.M. et al. (2014). New luminescence ages for the Galería Complex archaeological site: Resolving chronological uncertainties on the Acheulean record of the Sierra de Atapuerca, northern Spain. PLoS ONE, 9(10): e110169. **[4]** Bermúdez de Castro, J.M.; Rosas, A. (1992). A human mandibular fragment from the Atapuerca Trench (Burgos, Spain). Journal of Human Evolution, 22(1), 41–46. **[5]** Del Valle, H.; Rodríguez-Navarro, A.B.; Moclán, A. et al. (2025). Bone diagenesis and stratigraphic implications from Pleistocene karst systems. Scientific Reports, 15, 5496, 1–16. **[6]** Núñez-Lahuerta, C.; Galán, J.; Cuenca-Bescós, G. et al. (2022). A bird assemblage across the MIS 9/8 boundary: The Middle Pleistocene of Galería (Atapuerca). Quaternary Science Reviews, 293, 107708.